



Energy consumption investigation of a three-axis machine tool and ball-end milling process

Renjie Ge^{1,2} · Song Zhang^{1,2} · Renwei Wang^{1,2} · Xiaona Luan^{1,2} · Irfan Ullah^{1,2}

Received: 6 October 2021 / Accepted: 25 June 2022 / Published online: 14 July 2022
 © The Author(s), under exclusive licence to Springer-Verlag London Ltd., part of Springer Nature 2022

Abstract

The manufacturing industry consumes a considerable amount of energy every year, which poses a major challenge to resource consumption and environment problem. To overcome these difficulties, it is necessary to understand the machine tools' power characteristics. The current research aims to investigate the energy consumption of the machine tool and to establish a cutting power model for ball-end milling process. First, a cutting power theoretical model for a ball-end milling cutter was established based on the infinitesimal cutting force. Secondly, a series of experiments were conducted to reveal and validate the mathematical function of spindle power and feed power. Finally, slotting milling experiments were conducted, and a cutting power empirical model was proposed by analyzing the correlation between cutting forces and cutting power. The results showed that the spindle power, feed power, and cutting power could be exactly predicted by the proposed method. Furthermore, the Z-axis's feed power characteristic was revealed that the gravity made the Z-axis's motor transform to the generator when Z-axis moved in the downward direction. For cutting power model, the theoretical model and empirical model had the same predictive accuracy, while the empirical model had a simpler form and could be easier applied. The proposed power investigation method provided technical support for the research of the machine tools' energy consumption characteristics.

Keywords Energy consumption · Machine tool · Ball-end milling · Cutting power

Abbreviations

dF_t, dF_r, dF_a	Differential cutting forces in tangential, radial, and axial direction (N)	k	Axial position angle (rad)
K_{te}, K_{re}, K_{ae}	Edge-specific coefficients (N/mm)	α	Helix angle of the ball-end milling cutter (rad)
K_{ts}, K_{rs}, K_{as}	Shear-specific coefficients (N/mm ²)	θ	Angular position of the elemental cutter edge (rad)
dS	Differential length of cutting-edge (mm)	ψ	Angular position of the reference cutting edge (rad)
t_n	Instantaneous undeformed chip thickness (mm)	φ	Lag angle of the elemental edge (rad)
db	Differential width of chip (mm)	$O_c-X_cY_cZ_c$	Cutting tool coordinate system
R	Radius of the ball-end milling cutter (mm)	$O-XYZ$	Machine tool coordinate system
f_z	Feed per tooth (mm)	P	A point on the cutting edge
		$dF_{X_c}, dF_{Y_c}, dF_{Z_c}$	Differential cutting forces in X_c , Y_c , and Z_c direction (N)
		$\bar{F}_{X_c(Y_c,Z_c)}$	Mean cutting forces in X_c , Y_c , and Z_c direction (N)
		N	Total number of cutting edges
		θ_{st}, θ_{ex}	Cut-in and cut-out angular position of the elemental cutting edge (rad)
		k_{up}, k_{low}	Upper and lower bounds of the axial position angle (rad)
		P_c	Cutting power (kW)
		dF_f	Differential cutting force in feed direction (N)

✉ Song Zhang
 zhangsong@sdu.edu.cn

¹ Key Laboratory for High Efficiency and Clean Mechanical Manufacture of Ministry of Education, School of Mechanical Engineering, Shandong University, Jinan 250061, People's Republic of China

² Key National Demonstration Center for Experimental Mechanical Engineering Education, Shandong University, Jinan 250061, People's Republic of China

n	Spindle speed (r/min)
v_f	Feed rate (mm/min)
η	Coefficient considering the power loss of spindle transmission
a_p	Axial cutting depth (mm)
P_{SR}	Spindle power (kW)
P_X, P_Y	Feed power of X-axis and Y-axis (kW)
P_{Z-up}, P_{Z-down}	Feed power of the Z-axis in the upward direction and downward direction (kW)
R^2	Coefficient of determination
P_1	Cutting power calculated by theoretical model (kW)
P_2	Cutting power calculated by empirical model (kW)

1 Introduction

Nowadays, human civilization is tackled with environmental, energy, and population tribulations, among which energy is the most important. Saving energy and reducing emissions have attracted more and more attention. In 2020, the US Energy Information Administration report showed that world energy consumption will rise nearly 50% by 2050, and industry accounts for 38% of total energy consumption [1]. Computerized numerical control (CNC) machine tools are the basis of industrial manufacturing and critical energy consumption components [2]. A deep understanding of the power characteristics of CNC machine tools is helpful in two ways. On the one hand, energy consumption can optimize the processing parameters and make the processing green and clean [3, 4]. On the other hand, machine power can be used to predict additional machining information in the machining process, such as cutting forces [5], cutting tool wear [6], and surface roughness [7]. In addition, the power consumption can be easily measured without any influence on the machining process. Therefore, using power to predict other machining information can ensure the continuity of the machining [8].

According to the machine tool movement, the machine tool statuses can be divided into three kinds: standby status, air-cutting status, and cutting status. Standby status and air-cutting status are collectively referred to as non-cutting status. Based on the machine tool's status, the machine tool's total power is made up of three parts: basic power, air-cutting power (spindle power and feed power), and cutting power [9]. The machine tool's energy consumption in non-cutting status accounts for the main part of the power consumption [10].

Li et al. [11] measured the PL700 machine tool's energy consumption, and reported that the basic power accounts for 64% of the total machine tool's power. Denkena et al. [12] investigated the energy consumption of the DMU 340P

vertical machining center, reported that machine cooling, compress air, and cutting fluid supply accounts for 22%, 16%, 10% of the total machine tool's power, respectively. Most studies regard basic power as a constant, and the power of some auxiliary devices, such as cooling device, that operate intermittently is neglected, which will lead to the prediction error of machine tool energy consumption.

Hu et al. [13] used linear regression model to establish the relationship between spindle power and spindle speed, and Li et al. [14] established the relationship by quadratic regression model. These empirical models based on experimental results had a reliable prediction in practical application. Luan et al. [15] studied the CNC machine tool's power characteristics in non-cutting status. The authors reported that the spindle power was different under different transmission chains, even if the spindle speed was the same. Edem and Mativenga [16] pointed out that the weight of the load played a leading role in the power consumption compared with the feed rate, and the strategy that reducing the weight of worktable and workpiece was crucial to reduce the feed power and energy consumption. Liu et al. [17] reported negative feed power while analyzing the downward movement of the Z-axis. They pointed out that this occurred because some auxiliary equipment closed, but they did not provide the information about the auxiliary equipment.

As mentioned above, cutting power can reflect a lot of information when the machine tool is in cutting status. Therefore, many researches were carried out to investigate the cutting power model. Most of the cutting power models are established in two ways, material removal rate (MRR) and cutting force. Gutowski et al. [18] reported that the power during cutting is proportional to the volume of material removed per unit time. Zhou et al. [9] established cutting power based on MMR and spindle speed during face milling, and the model had a reliable accuracy. However, this theory cannot explain the phenomenon that different cutting parameters lead to different cutting power even if the MMR is the same. The power model based on cutting force combines cutting power with the actual machining process. Liu et al. [19] established a cutting power model based on milling force and pointed out that the total power consumption was a linear relationship of average cutting power. Luan et al. [20] established a cutting power model based on the infinitesimal cutting force during face milling HTCuCrSn-250 and additional load loss was considered in the model. Shi et al. [21] decomposed cutting power into the product of force and speed in both cutting speed and feed rate directions and established a reliable cutting power model. The ball-end milling cutter can process complex surfaces for aerospace and biomedical application, so it is of great significance to study the energy consumption in this machining process. Quintana et al. [22] considered spindle speed, feed rate, and other five factors as inputs and developed an artificial neural network to predict power consumption in high-speed ball-end

milling operations. Oda et al. [23] investigated the influence of tool-workpiece inclined angle on power consumption in five-axis machine tool during the ball-end milling process.

From the literature review, most studies on the machine tool’s power consumption are not comprehensive enough, especially for basic power and Z-axis feed power in downward direction. Besides, the correlation between cutting power and cutting forces in the X–Y–Z direction is not clear for the ball-end milling process. Therefore, in this research, the power consumption on a three-axis machine tool was investigated, including basic power, spindle power, and feed power. To reveal the relationship between the cutting power and cutting forces, series of slotting milling experiments were conducted. The proposed power model offers an accurate prediction of energy consumption, which can help manufacturers select appropriate process parameters to reduce energy consumption.

2 Methodology

2.1 Cutting power model

During the material removal process, the resistance of spindle rotation and feed movement increases. Therefore, the key to establishing a cutting power model is to calculate the cutting forces at the tooltip.

As demonstrated in Fig. 1, the differential cutting forces on an infinitesimal cutting edge can be expressed by Eq. (1) for a general milling process with a ball-end milling cutter [24].

$$\begin{cases} dF_t = K_{te} dS + K_{ts} t_n db \\ dF_r = K_{re} dS + K_{rs} t_n db \\ dF_a = K_{ae} dS + K_{as} t_n db \end{cases} \quad (1)$$

where dF_t , dF_r , dF_a (N) are the differential cutting forces in tangential, radial, and axial direction; K_{te} , K_{re} , K_{ae} (N/mm) are the edge-specific coefficients; K_{ts} , K_{rs} , K_{as} (N/mm²) are the shear-specific coefficients; the differential length of cutting-edge dS (mm), the instantaneous undeformed chip thickness t_n (mm), and the differential width of chip db (mm) can be expressed as [24]:

$$\begin{cases} dS = R\sqrt{1 + \sin^4 k \tan^2 \alpha} dk \\ t_n = f_z \sin k \sin \theta \\ db = R dk \\ \theta = \psi - \varphi \\ \varphi = \frac{(R - R \cos k) \tan \alpha}{R} \end{cases} \quad (2)$$

where R (mm) is the radius of the ball-end milling cutter; k (rad) is the axial position angle; α (rad) is the helix angle of the ball-end milling cutter; in this research, α is simplified as a fixed value; f_z (mm) is the feed per tooth; θ (rad) is the angular position of the elemental cutter edge; ψ (rad) is the

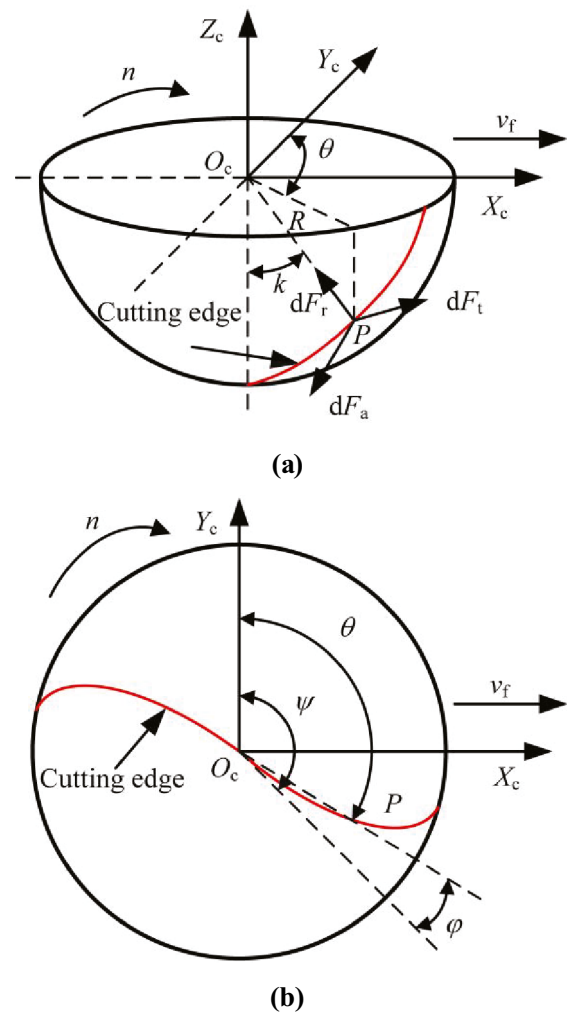


Fig. 1 Cutting forces for ball-end milling process: **a** schematic diagram of cutting forces (3D), and **b** schematic diagram of cutting forces (vertical view)

angular position of the reference cutting edge; φ (rad) is the lag angle of the elemental edge.

In Fig. 1, cutting tool coordinate system $O_c-X_cY_cZ_c$ is established. The origin O_c is placed at center of spherical part of the cutter. The Z_c -axis coincides with the cutter axis. The X_c -axis coincides with the feed direction of cutter. The Y_c -axis is determined by right-hand rule. And P is a point on the cutting edge. To obtain cutting forces in $O_c-X_cY_cZ_c$ coordinate, the forces in Eq. (1) are resolved as:

$$\begin{bmatrix} dF_{Xc} \\ dF_{Yc} \\ dF_{Zc} \end{bmatrix} = \begin{bmatrix} -\cos \theta & -\sin \theta \sin k & -\sin \theta \cos k \\ \sin \theta & -\cos \theta \sin k & -\cos \theta \cos k \\ 0 & \cos k & -\sin \theta \end{bmatrix} \begin{bmatrix} dF_t \\ dF_r \\ dF_a \end{bmatrix} \quad (3)$$

Similarly, the mean cutting forces in $O_c-X_cY_cZ_c$ coordinate can be resolved as follow:

Table 1 The main parameter of the MXR-460 V machine center

Item	Information
Dimension of worktable	460 mm × 1000 mm
X-axis stroke	762 mm
Y-axis stroke	460 mm
Z-axis stroke	450 mm
Spindle speed	50–8000 r/min (infinite speed variation)
Feed rate	1–30000 mm/min (X/Y/Z)
Fast feed rate	36 m/min (X/Y); 30 m/min (Z)

$$\bar{F}_{Xc(Yc, Zc)} = \frac{N}{2\pi} \int_{\theta_{st}}^{\theta_{ex}} \int_{k_{low}}^{k_{up}} dF_{Xc(Yc, Zc)} \quad (4)$$

where N is the total number of cutting edges; θ_{st} (rad) and θ_{ex} (rad) are the cut-in and cut-out angular position of the elemental cutting edge; k_{up} (rad) and k_{low} (rad) are the upper and lower bounds of the axial position angle.

Therefore, the instantaneous differential cutting power can be calculated as a sum of the differential cutting powers due to spindle rotation and feed axis movement:

$$dP_c = \frac{dF_t \cdot R \sin k}{1000} \times \frac{2\pi n}{60} + dF_f \times \frac{v_f}{60000} \quad (5)$$

where dF_f (N) is the differential force in feed direction; n (r/min) is spindle speed; v_f (mm/min) is feed rate.

The theoretical mean value of cutting power in a rotational period can be expressed as:

$$P_c = (1 + \eta) \frac{N}{2\pi} \int_{\theta_{st}}^{\theta_{ex}} \int_{k_{low}}^{k_{up}} \frac{dF_t \cdot R \sin k}{1000} \times \frac{2\pi n}{60} + \frac{N}{2\pi} \int_{\theta_{st}}^{\theta_{ex}} \int_{k_{low}}^{k_{up}} dF_f \times \frac{v_f}{60000} \quad (6)$$

where η is a coefficient considering the power loss of spindle transmission.

2.2 Experimental equipment

Power measurement experiments were conducted on a three-axis vertical machining center (MXR-460 V, OKUMA-BYJC, China). Table 1 lists the main parameters of the MXR-460 V machine center. A two-flute solid carbide ball-end milling cutter (JH970100-Tribon, Seco Company, Sweden) was used for milling experiments under dry cutting conditions. The cutter had a helix angle of 30° and a radius of

5 mm. The material of the workpiece was AISI P20 mold steel, whose chemical composition is listed in Table 2. The cutting force components were collected by a dynamometer (9257B, KISTLER, Switzerland). The electric power consumption of the machine was measured by a power analyzer (PW6001, HIOKI, Japan) at the back of the machine tool. Details of the experimental set-up are demonstrated in Fig. 2.

2.3 Experimental design

2.3.1 Experimental design of non-cutting status

Firstly, power data was recorded from the machine tool powering up to powering down, and the status of the machine tool's components, activated or closed, were also recorded.

Then, to reveal the relationship between spindle power and spindle rotating speed, 12 groups of experiments were designed based on spindle speed, ranging from 200 to 6800 r/min with an interval of 600 r/min. In every experiment, the spindle was controlled to rotate for 15 s, and the total power of the machine tool was recorded at stable status; then, the basic power was deducted to obtain the spindle power.

Besides, 10 groups of experiments were designed based on feed rate, ranging from 200 to 5600 mm/min with an interval of 600 mm/min, and the experiments were performed for all feed axes (i.e., X, Y, and Z). Due to the MXR-460 V machine tool's characteristic, the feed axes could move only when the spindle is rotating. Therefore, in every experiment, first, the spindle was controlled to rotate at 50 r/min for 10 s; then, the feed axis was controlled to move along a certain distance. As listed in Table 1, the spindle speed of the MXR-460 V machine center ranges from 50 to 8000 r/min. Generally, the higher the spindle speed, the greater the spindle power [9], so to reduce energy consumption, the spindle speed was set at 50 r/min in the feed power experiments.

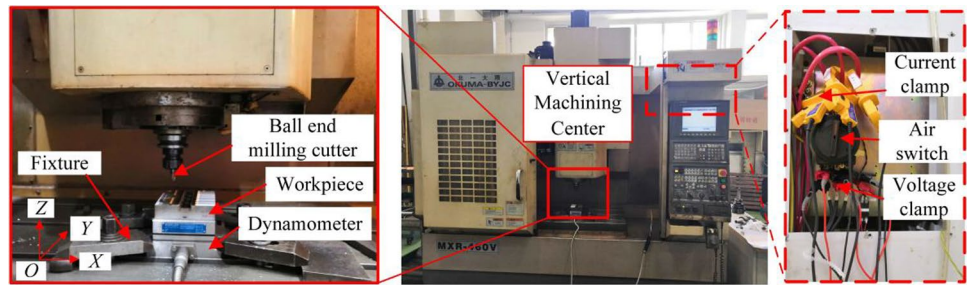
The range of spindle speed and feed rate is commonly used in practical machining. All the experiments were repeated twice to decrease the measurement error. The schematic diagram of the spindle and feed axis drive system in MXR-460 V is demonstrated in Fig. 3.

As shown in Fig. 3, MXR-460 V machine center directly drives the spindle by using a built-in driving motor, which combines the driving motor with the spindle to achieve direct drive without any intermediate links. And this driving mode can reduce the power loss caused by mechanical transmission friction. In X-axis, Y-axis, and Z-axis feed systems, the driving process is as follows. First, the driving motors drive the ball screw to rotate by using the coupling. Then, the ball

Table 2 Chemical composition of AISI P20 (wt%)

Ele	C	Si	Mn	P	Cr	Mo	S	Fe
Content	0.28~0.40	0.20~0.80	0.60~1.00	≤0.03	1.40~2.00	0.30~0.55	≤0.03	Bal.

Fig. 2 Experimental set-up

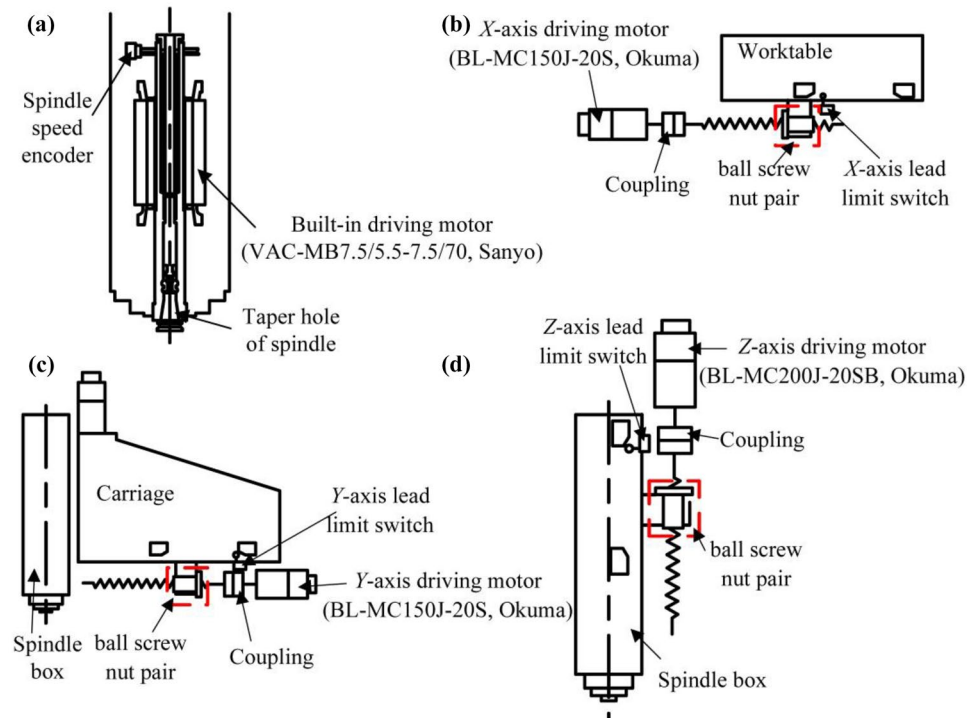


screw nut pair converts the rotating motion of the ball screw into the linear motion of the corresponding components. The lead limit switches are used to prevent each feed axis from moving over the stroke range. Notably, the X-axis and Y-axis driving motor models are the same, but their respective motion loads are not the same. The X-axis driving motor drives worktable to move, the Y-axis driving motor drives spindle box and carriage to move. And in the feed power experiments, there are no workpieces on the worktable.

2.3.2 Experimental design of slotting milling

To investigate the relationship between cutting forces and cutting power, and to calibrate the edge-specific coefficients and shear-specific coefficients, 10 slotting milling experiments were conducted. The schematic diagram for slotting milling and the experiments' details are shown in Fig. 4 and Table 3, respectively. The milling parameters (n , a_p , f_z , and v_f) were selected according to the user manual of the milling cutter and the practical machining experience of AISI P20 mold steel [25].

Fig. 3 Drive systems of machine tool: **a** schematic diagram of the spindle drive system, **b**, **c**, and **d** schematic diagrams of the X-axis, Y-axis, and Z-axis drive system, respectively



3 Results and discussion

3.1 The power during non-cutting status

3.1.1 Basic power

Figure 5 exhibits the power change of the machine tool from powered up to powered down: first, the machine tool powered up, and a fan activated, and basic power was 0.351 kW at that time; secondly, the screen activated and screen power was 0.048 kW; thirdly, light device activated, and light device power was 0.028 kW; then, control system and cooling device activated, and the cooling device was in preheating stage with the basic power was 2.002 kW; the cooling device activated and closed periodically, and the activating and closing time were about 0.63 min and 0.56 min, respectively; finally, control system closed and the machine tool powered down. And the stable basic power when the cooling device activated and closed was 2.018 kW and 1.571 kW, respectively. The basic power of the machine tool changed with the activating and

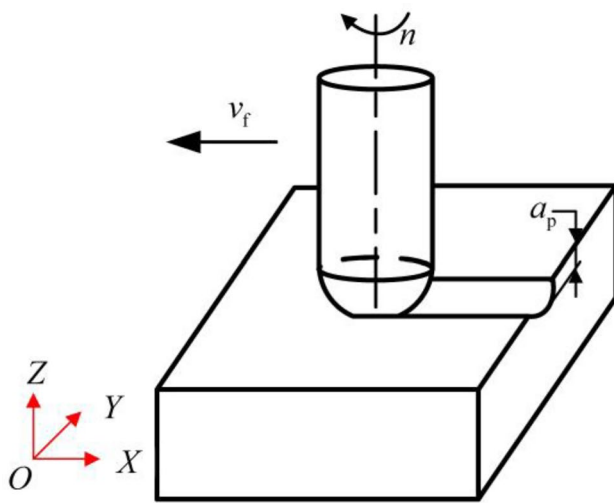


Fig. 4 Slotting milling diagram

closing of auxiliary devices, such as fan, light device, and cooling device. Because the cooling device activated and closed periodically, all the following experiments were conducted when the cooling device closed. If the cooling device is not closed, then the power of the cooling device should be removed from the experimental results.

3.1.2 Spindle power

Table 4 presents the experimental values of spindle power at different spindle speeds. The fitting curve of spindle power is shown in Fig. 6, and the fitting result ($R^2=0.99893$) was expressed as:

$$P_{SR} = 0.0382 + 2.60509 \times 10^{-5}n + 3.37302 \times 10^{-9}n^2 \quad (200 \leq n \leq 6800) \quad (7)$$

As shown in Fig. 6, the relationship between spindle power and spindle speed did not perform piecewise, as mentioned in reference [15]. The reason was that the spindle was only driven by a built-in drive motor. Therefore, the MXR-460 V machine tool only had one drive chain for the spindle.

Table 3 Experiment design of slot milling cutting (spindle speed was 3000r/min)

Experimental number	a_p (mm)	f_z (mm)	v_f (mm/min)
C01	0.8	0.1	600
C02	0.8	0.14	840
C03	1.6	0.1	600
C04	1.6	0.12	720
C05	2.4	0.1	600
C06	2.4	0.08	480
C07	3.2	0.1	600
C08	3.2	0.06	360
C09	4	0.1	600
C10	4	0.04	240

To verify the fitting result, five spindle speeds were randomly selected, which were 470, 1562, 3837, 5552, 6500r/min, respectively. Table 5 presents that the maximum relative error was 3.55%.

3.1.3 Feed power

Table 6 presents the experiment values of feed power at different feed rates. The fitting curves of feed power are shown in Fig. 7. The fitting result ($R^2=0.99494$) of the X-axis was expressed as:

$$P_X = 0.00104 + 9.55093 \times 10^{-6}v_f + 6.20791 \times 10^{-10}v_f^2 \quad (200 \leq v_f \leq 5600) \quad (8)$$

The fitting result ($R^2=0.99384$) of the Y-axis was expressed as:

$$P_Y = 0.00363 + 8.26557 \times 10^{-6}v_f + 1.4415 \times 10^{-9}v_f^2 \quad (200 \leq v_f \leq 5600) \quad (9)$$

The fitting result ($R^2=0.99984$) of the Z-axis in upward direction was expressed as:

$$P_{Z-up} = 0.04063 + 1.12576 \times 10^{-4}v_f \quad (200 \leq v_f \leq 5600) \quad (10)$$

The fitting result of the Z-axis in downward direction was expressed as:

$$P_{Z-down} = \begin{cases} -0.04223 - 6.68333 \times 10^{-5}v_f & (200 \leq v_f < 2000) \\ -0.17686 & (2000 \leq v_f \leq 5600) \end{cases} \quad (11)$$

Figure 7d shows that the feed power of the Z-axis in the downward direction was negative and different from others. The phenomenon was because that gravity acted as a driving force, and the electromagnetic force that made the spindle rotate acted as an obstructive force when the Z-axis moved in the downward direction. Therefore, the motor of the Z-axis was transformed into a generator [26] and inputted electrical energy into the grid, which decreased the total power of the machine tool. When the feed rate exceeded 2000 mm/min, the Z-axis's feed power in the downward direction stayed stable, which owed to the machine tool circuit that stabled the current to reduce the impact on electrical components. The demarcation point of 2000 mm/min depended on the structure of the circuit in a machine tool, especially the inductance, which resists the change of current.

Figure 7 shows that the Y-axis's feed power was bigger than that of the X-axis at the same feed rate, while the X-axis and Y-axis had the same motor model. It was because that the load gravity of the X-axis and Y-axis was different (demonstrated in Fig. 3).

Five feed rates, 360, 1200, 3400, 4260, and 6000 mm/min, were randomly selected to verify the fitting result.

Fig. 5 Power change curve of the machine tool from powered up to power down

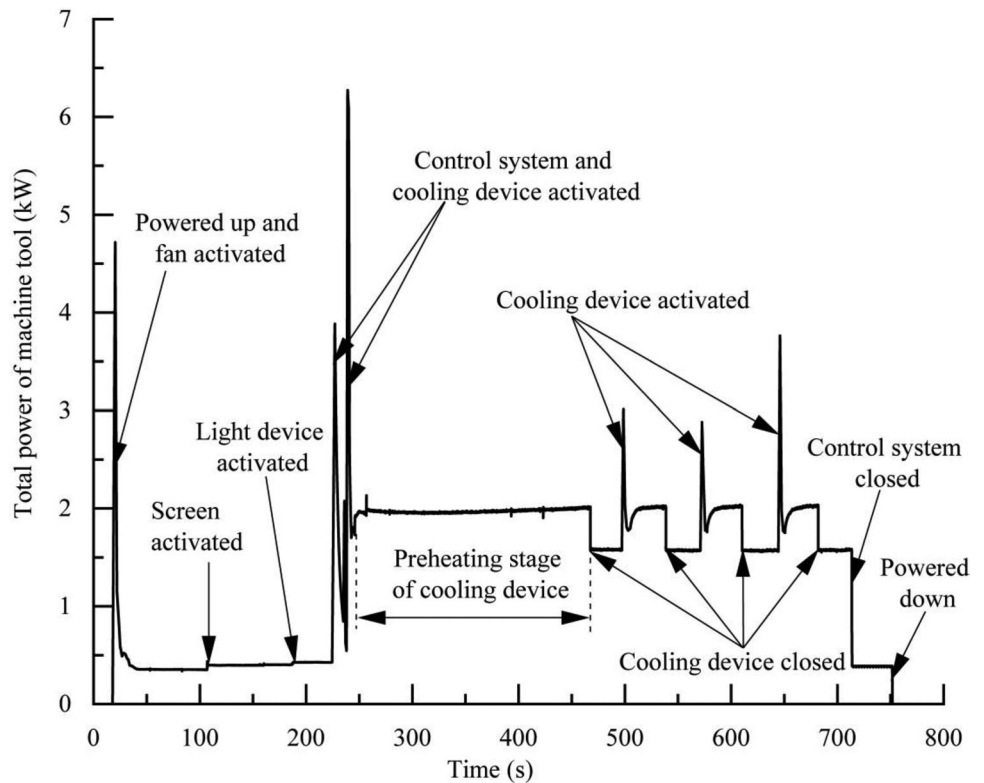


Table 7 shows that the maximum relative error of the feed power prediction was less than 10%.

3.2 Cutting power

Cutting force coefficients were calibrated by the least-square method and the method mentioned in the literature [27]. The calibration results were:

$$\begin{cases} K_{ts} = 1440.2 \times k^3 - 4887.6 \times k^2 + 5750.1 \times k - 4336.2, & K_{te} = -17.5 \\ K_{rs} = -2214.6 \times k^3 + 7377.8 \times k^2 - 7759.1 \times k + 3466.5, & K_{re} = 15.6 \\ K_{as} = -879.0 \times k^3 + 854.5 \times k^2 + 1646.0 \times k - 1104.1, & K_{ae} = 3.3 \end{cases} \quad (12)$$

The MXR-460 V machine tool used a built-in drive motor to directly drive spindle rotating, and the power loss of spindle transmission was too small. Therefore, η in Eq. (6) was zero, and the cutting power theoretical model could be expressed as,

Table 4 Experiment results of spindle power

n (r/min)	200	800	1400	2000	2600	3200
P_{SR} (kW)	0.045	0.061	0.085	0.099	0.126	0.155
n (r/min)	3800	4400	5000	5600	6200	6800
P_{SR} (kW)	0.185	0.218	0.255	0.296	0.332	0.365

$$P_1 = \frac{N}{2\pi} \int_{\theta_{st}}^{\theta_{ex}} \int_{k_{low}}^{k_{up}} \frac{dF_t \cdot R_{sink}}{1000} \times \frac{2\pi n}{60} + \frac{N}{2\pi} \int_{\theta_{st}}^{\theta_{ex}} \int_{k_{low}}^{k_{up}} dF_f \times \frac{v_f}{60000} \quad (13)$$

Figure 8 shows that the mean cutting forces in the X_c and Y_c direction changed consistently with the cutting power, while the mean cutting forces in the Z_c direction seemed nothing to do with cutting power. For example, for experimental numbers C01, C03, C05, C07, C09, as the cutting depth increased, the cutting power increased, and the mean cutting forces in X_c and Y_c direction also increased. In contrast, the mean cutting forces in the Z_c direction

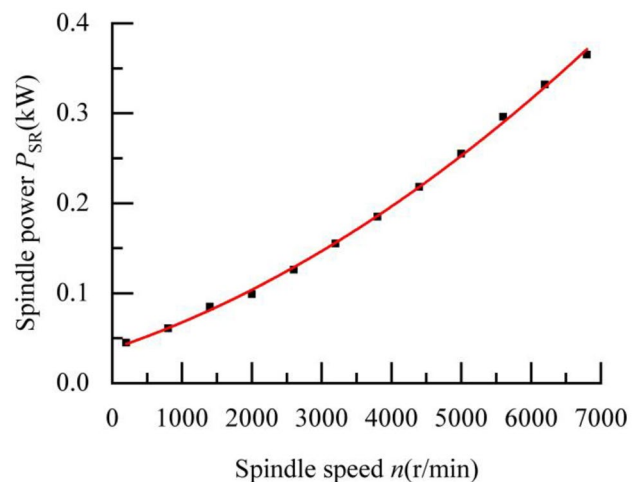


Fig. 6 Fitting curve of spindle power

Table 5 The prediction results of spindle power

n (r/min)	Experimental value (kW)	Predicted value (kW)	Relative error (%)
470	0.050	0.051	2.00
1562	0.085	0.087	2.35
3837	0.189	0.188	0.53
5552	0.297	0.287	3.37
6500	0.338	0.350	3.55

Table 7 The prediction results of feed power

Direction	v_f (mm/min)	Experimental value (kW)	Predicted value (kW)	Relative error (%)
X-axis	360	0.005	0.005	0
	1200	0.012	0.013	8.33
	3400	0.044	0.041	6.82
	4260	0.056	0.053	5.36
	6000	0.080	0.081	1.25
Y-axis	360	0.007	0.007	0
	1200	0.015	0.016	6.67
	3400	0.053	0.048	9.43
	4260	0.067	0.065	2.99
	6000	0.106	0.105	0.94
Z-axis upward	360	0.085	0.081	4.71
	1200	0.177	0.176	0.56
	3400	0.422	0.423	0.24
	4260	0.521	0.520	0.19
	6000	0.722	0.716	0.83
Z-axis downward	360	-0.066	-0.066	0
	1200	-0.133	-0.122	8.27
	3400	-0.178	-0.177	0.56
	4260	-0.174	-0.177	1.72
	6000	-0.176	-0.177	0.57

Table 6 Experiment results of feed power

v_f (mm/min)	P_X (kW)	P_Y (kW)	P_{Z-up} (kW)	P_{Z-down} (kW)
200	0.005	0.008	0.067	-0.053
800	0.007	0.009	0.131	-0.096
1400	0.015	0.016	0.195	-0.143
2000	0.022	0.026	0.267	-0.171
2600	0.029	0.036	0.331	-0.177
3200	0.040	0.042	0.399	-0.177
3800	0.049	0.060	0.466	-0.181
4400	0.053	0.067	0.536	-0.175
5000	0.064	0.083	0.608	-0.181
5600	0.074	0.093	0.671	-0.176

Fig. 7 Fitting curve of feed power: **a** feed power of X-axis, **b** feed power of Y-axis, **c** feed power of Z-axis in upward direction, and **d** feed power of Z-axis in downward direction

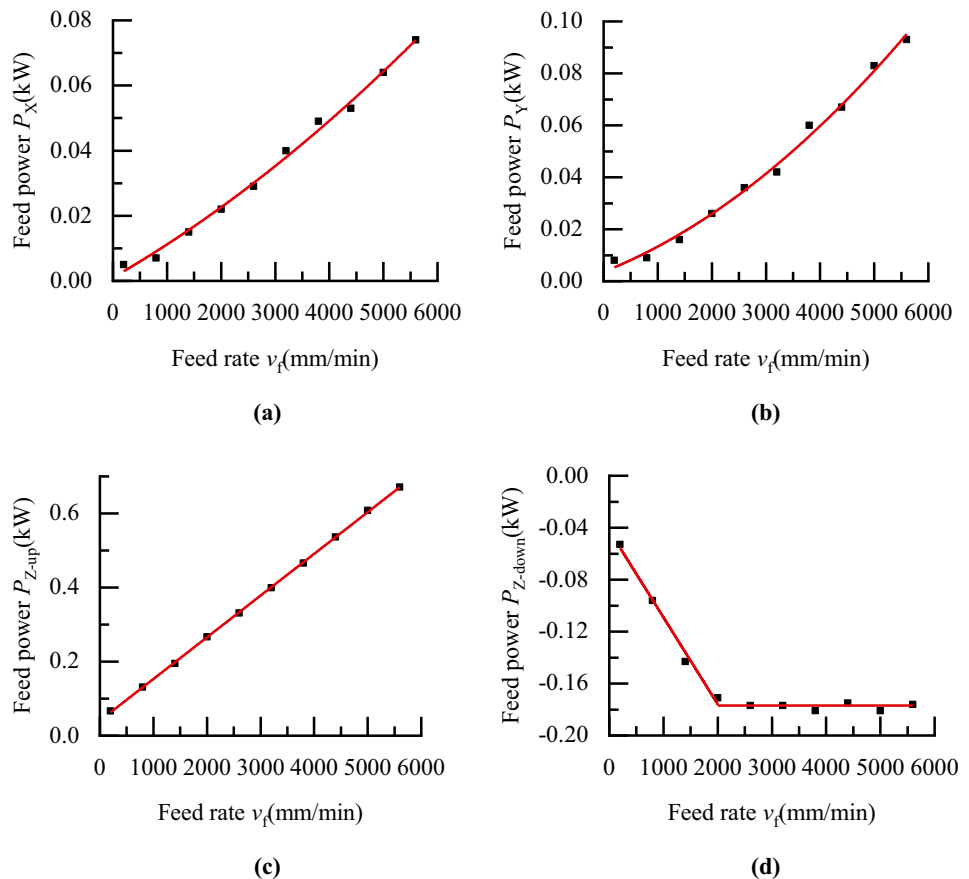
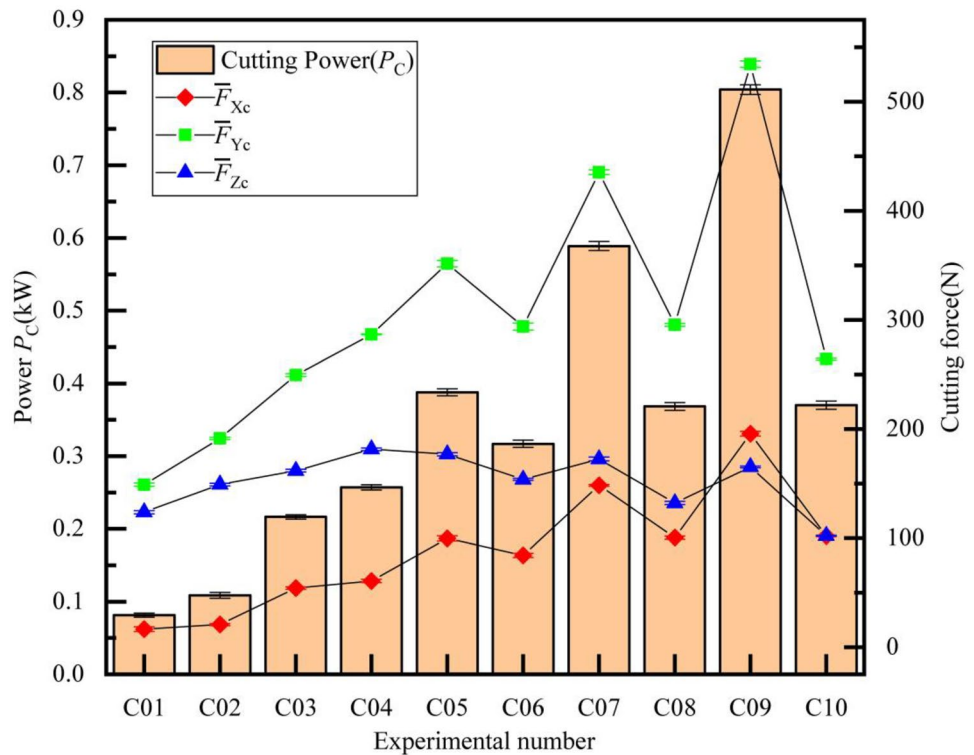


Fig. 8 Correlation between the mean cutting forces and cutting power



firstly increased, then decreased. The correlation coefficients between the mean cutting forces in X_c , Y_c , Z_c direction and cutting power were 0.99486, 0.97662, and 0.29413, respectively. The results showed that the cutting forces in the X_c and Y_c direction have a strong linear relationship with cutting power, while the linear relationship between cutting forces in the Z_c direction and cutting power is weak. The reasons for this phenomenon were that the cutting force in the X_c direction showed resistance to both the moving feed axis and the rotating spindle; similarly, the Y_c direction showed resistance to the rotating spindle. In contrast, the Z_c direction is not the resistance to the moving feed axis and the rotating spindle.

For the strong linear relationship between the mean cutting force in the X direction and cutting power, the fitting result ($R^2 = 0.99893$) between them was expressed as,

$$P_C = 4.21 \times 10^{-3} + 3.92 \times 10^{-3} \bar{F}_{Xc} \tag{14}$$

Therefore, a cutting power empirical model could be resolved by Eqs. (4) and (13) as,

$$P_2 = 4.21 \times 10^{-3} + 3.92 \times 10^{-3} \times \frac{N}{2\pi} \int_{\theta_{st}}^{\theta_{ex}} \int_{k_{low}}^{k_{up}} dF_{Xc} \tag{15}$$

Similarly, other slotting cutting experiments were conducted to prove the cutting power model. The predicted results are listed in Table 8. The average relative errors for Model 1 (the theoretical model) and Model 2 (the empirical model) were 6.66% and 5.51%, which showed that these models had the same acceptable accuracy. However, compared with Model 1, Model 2 had a simpler form and was

Table 8 The prediction results of cutting power (slot milling and spindle speed was 3000r/min)

Experimental number	a_p (mm)	f_z (mm)	Experimental value (kW)	P_1 (kW)	P_2 (kW)	Relative error (P_1) (%)	Relative error (P_2) (%)
V01	1.2	0.1	0.146	0.167	0.141	14.38	3.42
V02	1.2	0.12	0.167	0.194	0.154	16.17	7.78
V03	2	0.1	0.301	0.312	0.302	3.65	0.33
V04	2	0.08	0.252	0.261	0.262	3.57	3.97
V05	2.8	0.1	0.492	0.469	0.487	4.67	1.02
V06	2.8	0.06	0.31	0.313	0.342	0.97	10.32
V07	3.6	0.1	0.694	0.632	0.679	8.93	2.16
V08	3.6	0.04	0.312	0.315	0.359	0.96	15.06
Average	—	—	—	—	—	6.66	5.51

easier to be applied, for Model 2 only calculated cutting forces in one direction, and one double integral was needed.

4 Conclusions

This research investigated the power characteristics of a three-axis vertical machining center, including basic power, spindle power, and feed power. For cutting power, a theoretical model and an empirical model were established by different methods. The main conclusions were summarized as follows:

- The characteristics of spindle power and feed power were revealed by a mathematical function. It showed that gravity had an important influence on feed power. When the Z-axis moved downward, gravity made the Z-axis's motor transform to the generator, decreasing the total power consumption. Because of the different load gravity, even if the driving motor models of X-axis and Y-axis were the same, the feed power of Y-axis was bigger than that of X-axis at the same feed rate when there were no workpieces on the worktable.
- The cutting power theoretical model was established based on infinitesimal cutting force and the empirical model for slotting milling was established based on the strong linear relationship between the mean cutting forces and cutting power. Compared with the theoretical model, the empirical model had the same acceptable predictive accuracy. Moreover, the empirical model had a simpler form and was easier applied.
- The spindle power and feed power fitting models were verified in the three-axis vertical machining center, and the cutting power model was also verified in slotting milling AISI P20 with a ball-end milling cutter.

In the next step of this research, the proposed method will be expanded for different machine tools, cutters, workpiece materials, and machining methods.

Author contribution Renjie Ge provided the methodology, wrote the program code, investigated the experiments, and wrote the original manuscript. Song Zhang also provided the methodology, reviewed the manuscript, and provided the funding. Renwei Wang investigated the experiments and reviewed the manuscript. Xiaona Luan provided the methodology and reviewed the manuscripts. Irfan Ullah reviewed the manuscript. All authors have read and agreed to the published version of the manuscript.

Funding This work was supported by the National Natural Science Foundation of China (Grant No. 51975333), The National New Material Production and Application Demonstration Platform Construction Program (Grant No. 2020–370104-34–03-043952), and Taishan Scholar Project of Shandong Province (No. ts201712002).

Availability of data and material The authors declare that the data and material used or analyzed in the present study can be obtained from the corresponding author at reasonable request.

Code availability Custom code.

Declarations

Ethics approval Not applicable.

Consent to participate The authors declare that the involved researchers have been listed in the article, and all authors have no objection.

Consent for publication The authors confirm that the work has not been published before and does not consider other places. Its publication has been approved by all co-authors. Authors agree to publish the article in Springer's corresponding English-language journal.

Conflict of interest The authors declare no competing interests.

References

1. Energy Information Administration (EIA) (2020) International Energy Outlook 2020. Retrieved from <https://www.eia.gov/outlooks/ieo/pdf/ieo2020.pdf>. Last visited: 20 Jan 2021
2. Liu F, Wang QL, Liu GJ (2013) Content architecture and future trends of energy efficiency research on machining systems (in Chinese). *J Mech Eng* 49(19):87–94. <https://doi.org/10.3901/JME.2013.19.087>
3. Li L, Deng XG, Zhao JH, Zhao F, Sutherland JW (2018) Multi-objective optimization of tool path considering efficiency, energy-saving and carbon-emission for free-form surface milling. *J Clean Prod* 172:3311–3322. <https://doi.org/10.1016/j.jclepro.2017.07.219>
4. Fujishima M, Mori M, Oda Y (2014) Energy-efficient manufacturing on machine tools by machining process improvement. *Prod Eng Res Dev* 8:217–224. <https://doi.org/10.1007/s11740-013-0492-0>
5. Javorek B, Fuisseil BK, Jerard RB (2009) Calibration of a milling force model using feed and spindle power sensors. *Proc ASME Int Manuf Sci Eng Conf MSEC2008* 2:1–10. https://doi.org/10.1115/MSEC_ICMP2008-72315
6. Shao H, Wang HL, Zhao XM (2004) A cutting power model for tool wear monitoring in milling. *Int J Mach Tools Manuf* 44:1503–1509. <https://doi.org/10.1016/j.ijmactools.2004.05.003>
7. Liu N, Wang SB, Zhang YF, Lu WF (2016) A novel approach to predicting surface roughness based on specific cutting energy consumption when slot milling Al-7075. *Int J Mech Sci* 118:13–20. <https://doi.org/10.1016/j.ijmecsci.2016.09.002>
8. Liu PJ, Liu F, Qiu H (2017) A novel approach for acquiring the real-time energy efficiency of machine tools. *Energy* 121:524–532. <https://doi.org/10.1016/j.energy.2017.01.047>
9. Zhou LR, Li JF, Li FY, Xu XS, Wang LM, Wang G, Kong L (2017) An improved cutting power model of machine tools in milling process. *Int J Adv Manuf Technol* 91:2383–2400. <https://doi.org/10.1007/s00170-016-9929-x>
10. Zhou LR, Li JF, Li FY, Meng Q, Li J, Xu XS (2016) Energy consumption model and energy efficiency of machine tools: a comprehensive literature review. *J Clean Prod* 112:3721–3734. <https://doi.org/10.1016/j.jclepro.2015.05.093>
11. Li YF, He Y, Wang Y, Yan P, Liu XH (2014) A framework for characterising energy consumption of machining manufacturing

- systems. *Int J Prod Res* 52:314–325. <https://doi.org/10.1080/00207543.2013.813983>
12. Denkena B, Abele E, Brecher C, Dittrich MA, Kara S, Mori M (2020) Energy efficient machine tools. *CIRP Ann* 69(2):646–667. <https://doi.org/10.1016/j.cirp.2020.05.008>
 13. Hu LK, Peng C, Evans S, Peng T, Liu Y, Tang RZ, Tiwari A (2017) Minimising the machining energy consumption of a machine tool by sequencing the features of a part. *Energy* 121:292–305. <https://doi.org/10.1016/j.energy.2017.01.039>
 14. Li CB, Chen XZ, Tang Y, Li L (2017) Selection of optimum parameters in multi-pass face milling for maximum energy efficiency and minimum production cost. *J Clean Prod* 140:1805–1818. <https://doi.org/10.1016/j.jclepro.2016.07.086>
 15. Luan XN, Zhang S, Chen J, Li G (2019) Energy modelling and energy saving strategy analysis of a machine tool during non-cutting status. *Int J Prod Res* 57:4451–4467. <https://doi.org/10.1080/00207543.2018.1436787>
 16. Edem IF, Mativenga PT (2016) Impact of feed axis on electrical energy demand in mechanical machining processes. *J Clean Prod* 137:230–240. <https://doi.org/10.1016/j.jclepro.2016.07.095>
 17. Liu FY, Li XQ, Li YL, Wang ZJ, Zhai WD, Li FY, Li JF (2020) Modelling of the effects of process parameters on energy consumption for incremental sheet forming process. *J Clean Prod* 250:119456. <https://doi.org/10.1016/j.jclepro.2019.119456>
 18. Gutowski TG, Branham MS, Dahmus JB, Jones AJ, Thiriez A, Sekulic DP (2009) Thermodynamic analysis of resources used in manufacturing processes. *Environ Sci Technol* 43:1584–1590. <https://pubs.acs.org/doi/10.1021/es8016655>
 19. Liu N, Zhang YF, Lu WF (2015) A hybrid approach to energy consumption modelling based on cutting power: a milling case. *J Clean Prod* 104:264–272. <https://doi.org/10.1016/j.jclepro.2015.05.049>
 20. Luan XN, Zhang S, Li G (2018) Modified power prediction model based on infinitesimal cutting force during face milling process. *Int J Precis Eng Manuf-Green Technol* 5:71–80. <https://doi.org/10.1007/s40684-018-0008-7>
 21. Shi KN, Ren JX, Wang SB, Liu N, Liu ZM, Zhang DH, Lu WF (2019) An improved cutting power-based model for evaluating total energy consumption in general end milling process. *J Clean Prod* 231:1330–1341. <https://doi.org/10.1016/j.jclepro.2019.05.323>
 22. Quintana G, Ciurana J, Ribatallada J (2011) Modelling power consumption in ball-end milling operations. *Mater Manuf Process* 26(5):746–756. <https://doi.org/10.1080/10426910903536824>
 23. Oda Y, Mori M, Ogawa K, Nishida S, Fujishima M, Kawamura T (2012) Study of optimal cutting condition for energy efficiency improvement in ball end milling with tool-workpiece inclination. *CIRP Ann Manuf Technol* 61(1):119–122. <https://doi.org/10.1016/j.cirp.2012.03.034>
 24. Lee P, Altıntaş Y (1996) Prediction of ball-end milling forces from orthogonal cutting data. *Int J Mach Tools Manuf* 36:1059–1072. [https://doi.org/10.1016/0890-6955\(95\)00081-X](https://doi.org/10.1016/0890-6955(95)00081-X)
 25. Wang RW, Zhang S, Ge RJ, Luan XN, Wang JC, Lu SL (2021) Modified cutting force prediction model considering the true trajectory of cutting edge and in-process workpiece geometry in ball-end milling operation. *Int J Adv Manuf Technol* 115:1187–1199. <https://doi.org/10.1007/s00170-021-07285-y>
 26. Li FH, Wang Y (2012) *Fundamentals of motor and dyve* (in Chinese). Tsinghua University Press, Beijing, China
 27. Wei ZC, Wang MJ, Zhu JN, Gu LY (2011) Cutting force prediction in ball end milling of sculptured surface with Z-level contouring tool path. *Int J Mach Tools Manuf* 51:428–432. <https://doi.org/10.1016/j.ijmactools.2011.01.011>

Publisher's Note Springer Nature remains neutral with regard to jurisdictional claims in published maps and institutional affiliations.